Graphical Interpretation of the Extended Kalman Filter: Estimating the State-of-Charge of a Lithium Iron Phosphate Cell

Florin CIORTEA, Marian NEMES, Sorin HINTEA
Technical University of Cluj-Napoca, 400114, Romania
ciorteaflorin@yahoo.com

***Abstract*—Electric vehicles (EVs) fall in line with a new ideology of less waste and more conscious usage of resources, slowly picking up speed. In this context, energy storage is of paramount importance, making batteries a key element in the architecture of the electric vehicles. The state of the battery pack must be thoroughly monitored to prolong lifetime and extend vehicle range. For this, measurable physical quantities (i.e. terminal voltage, charge/discharge current, temperature) must be monitored and processed, while the inferred parameters (e.g. state-of-charge (SoC), state-of-health (SoH)) are computed and continuously updated. Whether we are talking about control of a noisy system, ill-defined decision-making processes or data analysis, estimation theory comes into play on a regular basis. The estimation algorithm is critical for appropriate usage of all available power, therefore, research effort is required to allow development of an optimum for a given application, by exploring design alternatives and their effects. This paper evaluates graphically an extended Kalman filter (EKF) for determining the SoC of lithium-ion batteries (LIBs) considering various cell models, initial conditions and charge/discharge profiles. The results are qualitatively and quantitatively assessed by extracting and visualizing the dynamics of the internal variables of the filter during operation.**

***Index Terms*—battery management systems, electric vehicles, Kalman filters, Lithium batteries, parameter estimation.**

I. INTRODUCTION

As the internal combustion engine (ICE) vehicle is a stable market, with fewer prospects of game-changing improvements, future development trends target alternative transportation solutions. Electric vehicles (EVs) play an important role in sustainable mobility thanks to high energy efficiency and zero-emissions when in use. Moreover, many of the countries that acknowledge climate change promote projects to drastically reduce harmful emissions and improve fuel efficiency for new vehicles [1]. The rising popularity of EVs led to new battery chemistries, capable of high energy densities, while satisfying the increasingly stringent safety requirements [2]. To meet EV specific power demands, series/parallel cell assemblies are organized in customized scalable modules, enabling design and service flexibility [3]. As batteries of the same chemical and physical characteristics differ in terms of performance parameters (e.g. capacity, internal resistance), charge imbalance is likely to occur within the module, especially during erratic usage. The nonuniformity of elements in a stack poses various problems, from performance limitation (e.g. the capacity of the entire string is restricted by the lowest capacity cell in the string) to safety concerns [4-5], thus battery management systems (BMS) for cell balancing come in handy [6]. The main input parameter driving the system is the state-of-charge (SoC) of the batteries, which gauges the amount of available charge relative to the nominal capacity of each cell. As the SoC of the battery represents a condition rather than a measurable quantity, its precise deduction is a real challenge for engineers. Several estimation methods were proposed throughout industry, ranging from plain, but less effective solutions (e.g. integration of charge/discharge current [7]), to more efficient, yet computationally heavy algorithms (e.g. nonlinear variants of the Kalman filter (KF) [8-10]). The growing computing power of automotive grade MCU families allows running of highly-advanced applications, ergo intricate solutions become progressively approachable.

While an ideal capacitor develops charge on its plates linearly with the voltage applied across it (i.e. $Q = C \cdot V$), lithium ion batteries (LIBs) pose a highly nonlinear open circuit voltage (OCV) vs. SoC characteristic (Fig. 1). Hence, the BMS needs its SoC estimator to be able to deal with the nonlinear behavior of the battery. The extended Kalman filter (EKF) [11] puts forth a means to handle nonlinearities while speculating the main benefit of its linear peer: the inherent predictor-corrector mechanism. Albeit not optimal, the EKF provides a potential solution for a variety of tasks, from tracking of moving objects [12-13] to control and decision-making systems or energy management [14-16].

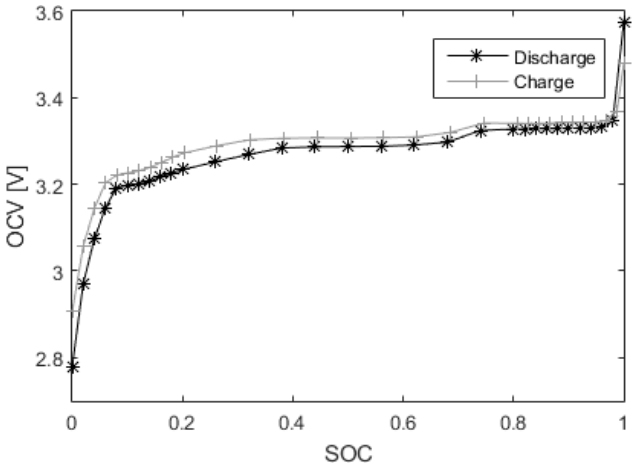

Figure 1. OCV vs. SoC characteristic far a $LiFePO_4$ battery after one hour resting period after each applied load pulse

Digital Object Identifier 10.4316/AECE.2018.03005

II. The Equivalent Circuit Battery Model

To perform properly, the estimator requires a precise battery model to mimic the physical behavior of the part, viz. to relate the measurable quantities to the available charge. Fig. 2 illustrates a 2nd order RC equivalent circuit model (ECM) and the typical voltage response of LIBs to a discharge current pulse. The transient response of the battery has two components, a fast one and a sluggish one, emulated by R_1C_1 and R_2C_2, respectively. The purely resistive component, R_0, relates any sudden change in the load profile to the steep edges of the measured voltage. As one can notice, once the battery has reached chemical equilibrium (i.e. $V_{R1C1} = V_{R2C2} = 0$) the OCV and terminal voltage are similar ($V_t = OCV$).

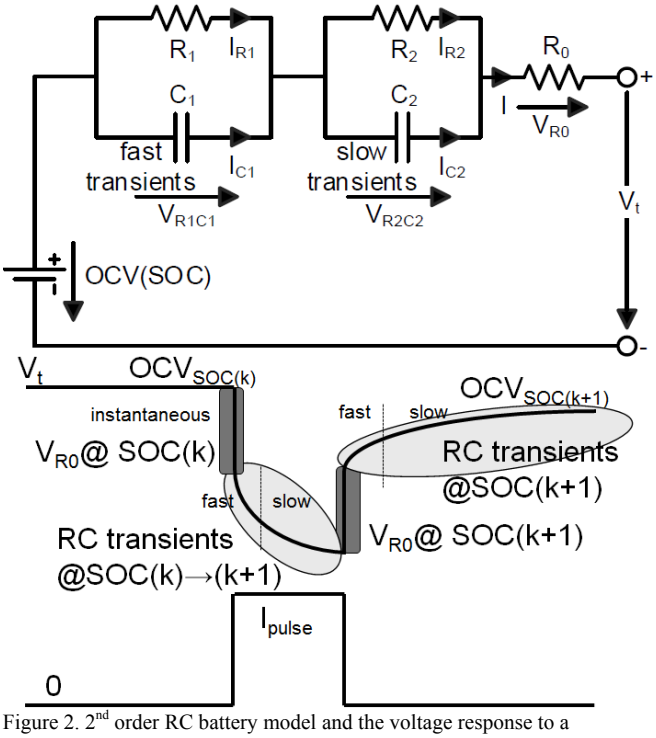

Figure 2. 2nd order RC battery model and the voltage response to a discharge current pulse

Besides offering an intuitive alternative to mathematical models [17], ECMs provide a set of equations, depicting the operation of the circuit (i.e. Kirchhoff's current (1) and voltage (2) laws), which are relatively easy to integrate into the structure of the filter, once discretized [18].

$$dV_{R_iC_i}/dt = -V_{R_iC_i}/(R_iC_i) + I/C_i \tag{1}$$

$$OCV(SoC) - V = \sum_{i=1}^{n} V_{R_iC_i} + IR_0 \tag{2}$$

As the above circuit state equations do not provide any direct insight on the battery's SoC, an additional relationship (i.e. Coulomb counting (3)) is required to plug-in the parameter into the structure of the estimation algorithm:

$$SoC(t+\Delta t) = SoC(t) - \frac{1}{C_n}\int_{t}^{t+\Delta t} \eta I(t)dt \tag{3}$$

where:

- $SoC(t)$ represents the battery SoC at initial time t;
- C_n is the nominal capacity of the part [A·h];
- $I(t)$ is the load current (positive for discharge) [A];
- η is the Coulombic efficiency (unity for discharge).

III. The Extended Kalman Filter Estimator

Fig. 3 shows a complete one-step-forward Kalman filtering cycle. The specific equations are organized in two distinct steps:

- the prediction (*a priori*) step, forecasts the mean value of the state vector (..., x^p_{k+1}, ...) and error covariance matrix estimates (..., P^p_{k+1}, ...) at each time index (..., $k+1$, ...). This is done according to the process model and by accounting for the measurement update during the previous time index: $x^p_{k+1} \leftarrow x^o_k$;
- the correction (*a posteriori*) step, adjusts the previous estimation based on measured data, such that a new, improved state (..., x^o_{k+1}, ...) will be propagated through the algorithm.

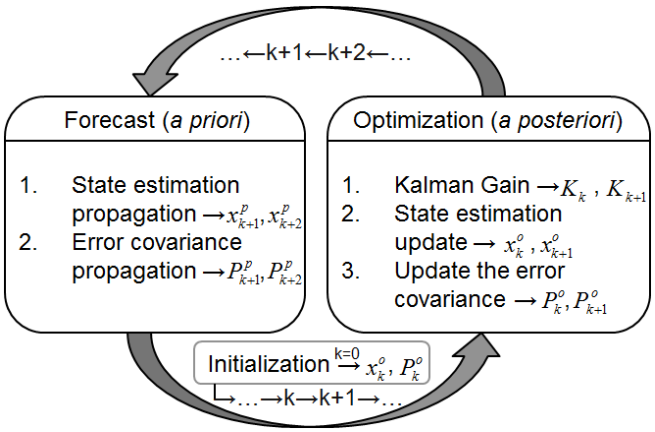

Figure 3. The Kalman filter algorithm diagram

The EKF process (4) and output (5) models are driven by the nonlinear, differentiable vector functions, $f(\cdot)$ and $g(\cdot)$, where x_{k+1} is the unknown system state vector at time index $k+1$, y_k depicts the observation or output vector, u_k is the control vector and the random variables w_k and v_k (6) represent the process and measurement additive, zero-mean noise samples. The two noise signals are uncorrelated, with covariance matrices Q and R, respectively.

$$x_{k+1} = f(x_k, u_k) + w_k \tag{4}$$

$$y_k = g(x_k, u_k) + v_k \tag{5}$$

$$w_k \sim N(0, Q), v_k \sim N(0, R) \tag{6}$$

$f(\cdot)$ and $g(\cdot)$ are linearized about each sample point by Taylor series expansion, taking into account only the first-order terms, also known as Jacobians. These terms are mathematically expressed in (7), where A_k, C_k represent the first partial derivatives of $f(\cdot)$ and $g(\cdot)$ with respect to x_k, whereas B_k, D_k are the Jacobian matrices of the same functions with respect to u_k. A detailed derivation of the Jacobians is done in [18].

$$A_k = \frac{\partial f(x_k, u_k)}{\partial x_k}, B_k = \frac{\partial f(x_k, u_k)}{\partial u_k}$$
$$C_k = \frac{\partial g(x_k, u_k)}{\partial x_k}, D_k = \frac{\partial g(x_k, u_k)}{\partial u_k} \tag{7}$$

The estimator starts running relying on the initial state (8) and error covariance (9) information available at step zero. Even though the Kalman filter turns out to be robust when poorly initialized, a proximal to reality input will reduce the

number of steps required to converge towards the real value.

Pursuant to the aforementioned process and algorithm diagram, the estimation steps are mathematically described below:

Initialization:

$$x_0^o = \mathrm{E}[x_0] \tag{8}$$

$$P_0^o = \mathrm{E}\left[(x_0 - x_0^o)(x_0 - x_0^o)^T\right] \tag{9}$$

Prediction:

$$x_{k+1}^p = f\left(x_k^o, u_k\right) = A_k x_k^o + B_k u_k \tag{10}$$

$$P_{k+1}^p = A_k P_k^o A_k^T + Q \tag{11}$$

Update:

$$K_{k+1} = P_{k+1}^p C_{k+1}^T \left(C_{k+1} P_{k+1}^p C_{k+1}^T + R\right)^{-1} \tag{12}$$

$$x_{k+1}^o = x_{k+1}^p + K_{k+1}\left[y_{k+1} - \overbrace{\left(C_{k+1} x_{k+1}^p + D_{k+1} u_{k+1}\right)}^{y_{k+1}^p = g\left(x_{k+1}^p, u_{k+1}\right)}\right] \tag{13}$$

$$P_{k+1}^o = \left(I - K_{k+1} C_{k+1}\right) P_{k+1}^p \tag{14}$$

The performance of the filter is strongly influenced by the ability of the ECM to closely emulate the real behavior of the battery. An adaptive battery model keeps track of its parameters over the entire SoC interval, hence boosting the model accuracy. Fig. 4 plots the extracted parameters of the ECM and their corresponding fit functions across the SoC interval for a 2nd order RC battery model, as in [19]. Subsequently, the derived curve fitting equations will be integrated into the structure of the estimator.

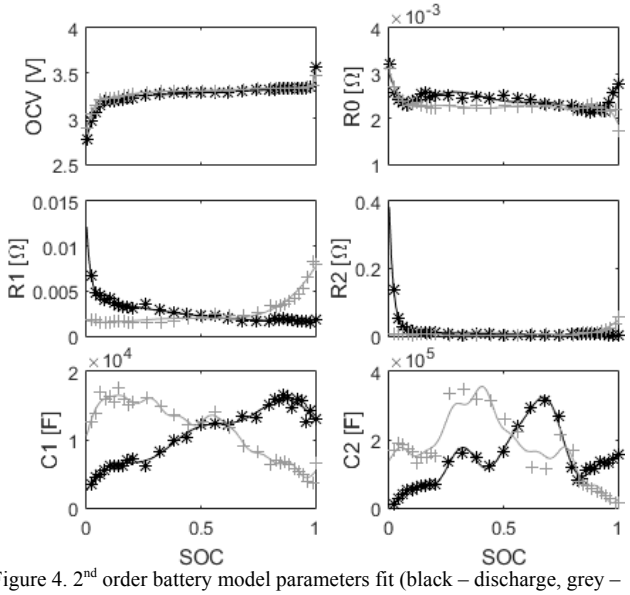

Figure 4. 2nd order battery model parameters fit (black – discharge, grey – charge)

The initial state vector accounts for a half-depleted battery and no voltage drop across the two RC branches → the battery is in chemical equilibrium (15). Also, the initial error covariance matrix was chosen as in (16), but only for the sheer pulsed charge/discharge patterns (Fig. 5).

$$x_0^o = \begin{bmatrix} 0.5 & 0 & 0 \end{bmatrix}^T \tag{15}$$

$$P_0^o = diag\begin{bmatrix} 1, & 0.01, & 0.01 \end{bmatrix} \tag{16}$$

The Q matrix is a rather holistic parameter which includes all modeling errors (unknown errors inclusively). Large values of Q show that the picked model performs poorly in predicting the process. On the other hand, R acts like a weighting factor on the contribution of the measurements to the estimation. A small R means that the measurements are close to reality, therefore reliable. Out of the two parameters, the filter performance is more responsive to the error covariance matrix of the process, Q. For this application Q and R were empirically determined:

$$R = \begin{bmatrix} 0.1 \end{bmatrix} \tag{17}$$

$$Q = diag\begin{bmatrix} 0.00001, & 0.001, & 0.001 \end{bmatrix} \tag{18}$$

Once implemented, the EKF application was validated against real data, using the same load profiles as for ECM parameterization in [19] in a first instance (i.e. 30 pulses of 19.5A each: 10/2% of SOC → 10/6% of SOC → 10/2% of SOC, Cn = 19.5Ah) – see Fig. 5 for discharge pattern.

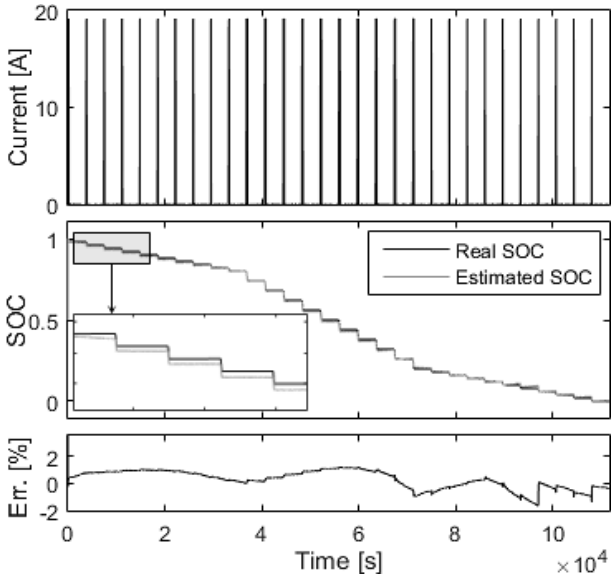

Figure 5. EKF performance – discharge pattern (one hour resting span)

Subsequently, the filter performance was confirmed against two random load profiles, accounting for an initially fully charged and a pre-discharged sample, as per Fig. 6 and Fig. 7, respectively.

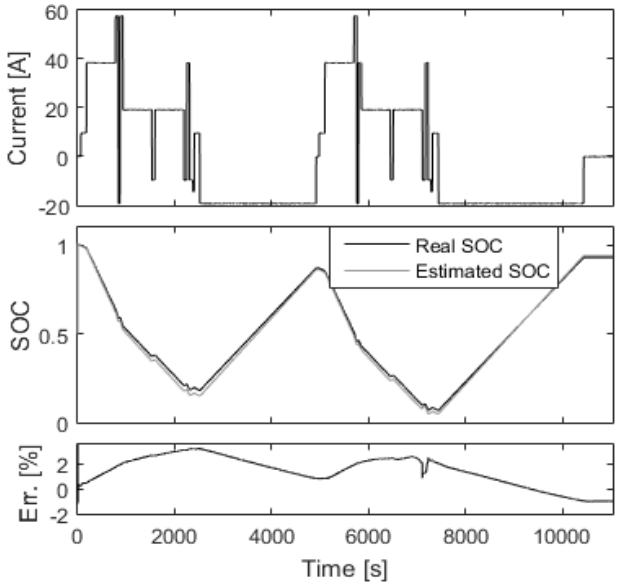

Figure 6. EKF performance – random load profile (fully charged battery)

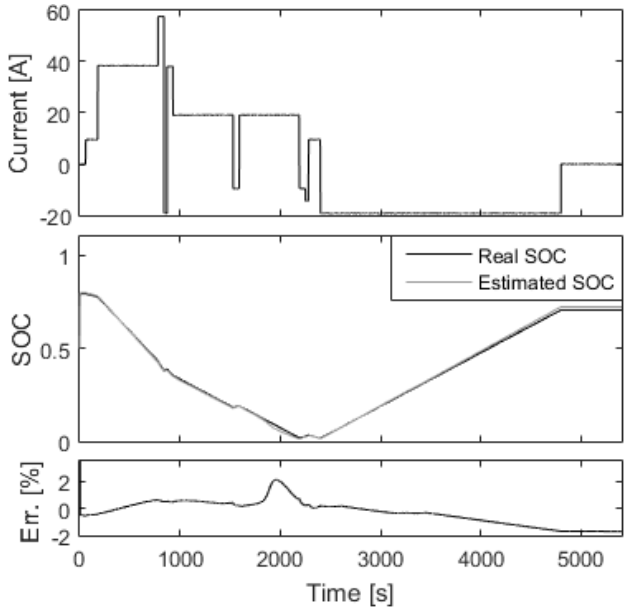

Figure 7. EKF performance – random load profile (pre-discharged battery)

As can be seen, the filter performed properly during any of the three applied load patterns, displaying a maximum error slightly below 3%, in relation to the random profile pictured in Fig. 6.

IV. EKF TUNING

A. EKF generic parameters

Besides the circuit model of the battery, the estimation accuracy is strongly influenced by the initial values of the state vector (x^o_0) and error covariance matrix (P^o_0). All the examples in this paper consider an initially half depleted cell at chemical equilibrium in terms of the state vector. Fig. 8 points out the effect of different initial error covariance matrices on the performance of the filter when a random load profile is applied to a partially pre-discharged battery. The convergence of the filter towards the real SoC value is strongly dependent on this matrix.

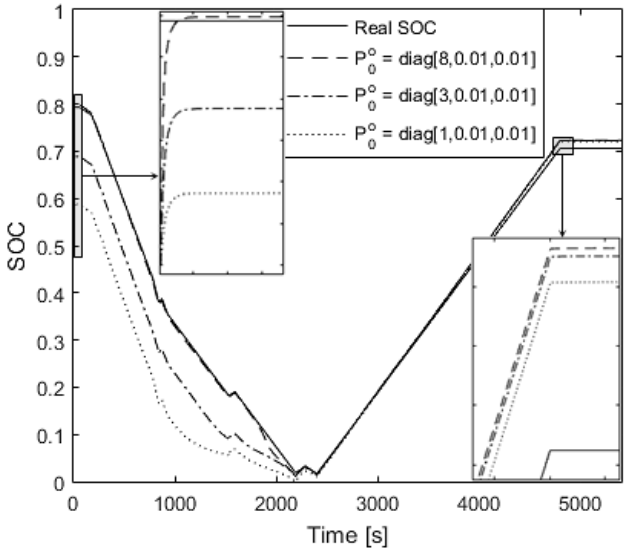

Figure 8. The effect of the initial covariance matrix on estimation quality

The elements of the initial error covariance matrix, P^o_0, affect the performance of the filter, mainly at start-up, but with considerable impact over the entire load profile. According to the process and observation models, the estimator will consider the prediction as being correct, even if not the case, and will rely mostly on the current integration from then on (Fig. 9). Basically, the estimator follows closely the real SoC shape relying solely on the Coulomb counting feature, but with a gap determined by the time it takes for the estimated terminal voltage to match the real one, as illustrated in the enlarged portions of Fig. 9.

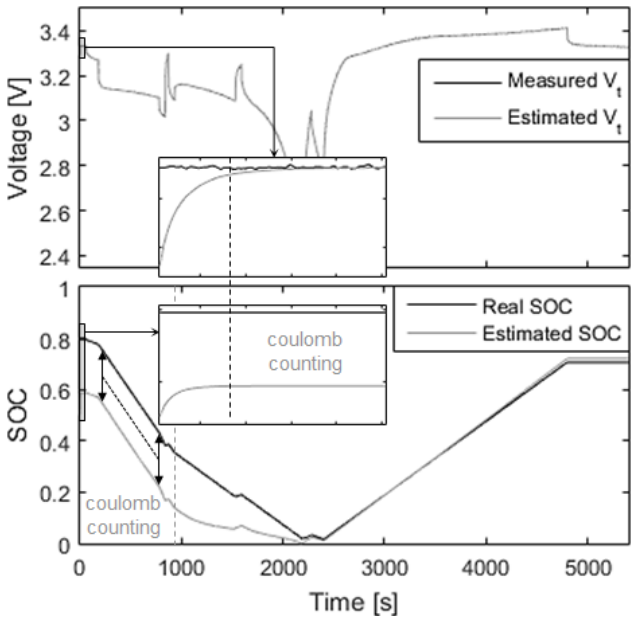

Figure 9. The relationship between the convergence of estimated and measured voltage and locking of estimated SoC (P^o_0=*diag[1,0.01,0.01]*)

The process and measurement error covariance matrices, Q and R respectively, pose a serious impact on the performance of the EKF and are rather difficult to determine optimally [20-21]. Hence, not seldom, it is more convenient to find their elements by trial and error, than to compute them. The top window in Fig. 10 shows the evolution of the filter when running two different values of Q, whereas the bottom one plots the same effect due to R (only one matrix was handled at a time, to isolate their impact on the filter). As noticed, both matrices influence radically the operation of the filter and moderate shifts in their values result in serious performance degradation.

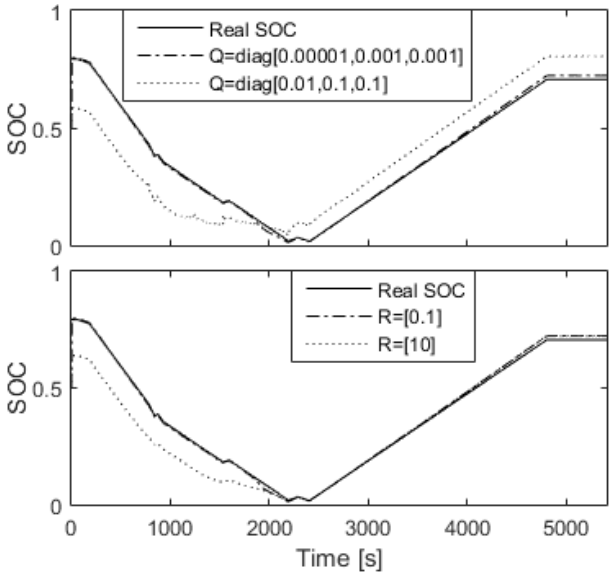

Figure 10. The impact of the matrices Q and R on the estimation accuracy

B. Application specific parameters

One other critical aspect, to be mentioned when running the estimator, is the OCV hysteresis effect due to insufficient resting after a charge/discharge event. As depicted in Fig. 11, the charge-discharge OCV hysteresis is decreasing with the relaxation period, although for $LiFePO_4$ olivine there is not much of a difference between relaxation intervals of five minutes or one hour, relative to the OCV value.

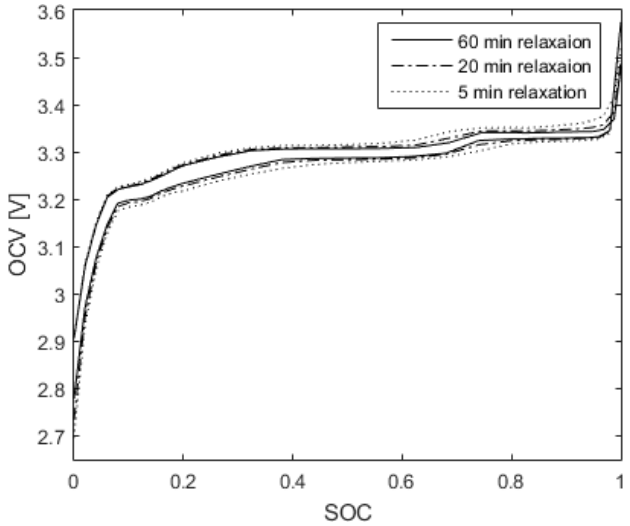

Figure 11. OCV charge-discharge hysteresis dynamics with the relaxation period

The hysteresis effect is more visible for lower SoC values, as a higher relaxation time is required for the battery to achieve chemical equilibrium. When running the filter this will come out as abrupt overturns in the estimated signal, causing severe deviations relative to the reference trace, as displayed in Fig. 12, and conversely altering the overall performance of the filter.

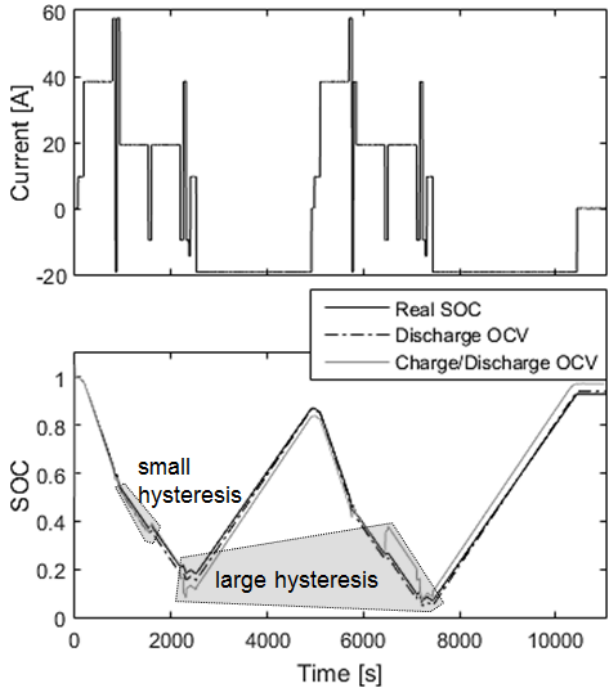

Figure 12. OCV hysteresis effects on SoC estimation

To eliminate the inconveniences due to OCV hysteresis, only one OCV fit expression was employed within the EKF structure, without discerning between charge/discharge events. The discharge OCV function in (19) was considered most appropriate, as during normal operation the battery will mostly discharge, excepting seldom circumstances like braking or coasting when energy is recovered by the vehicle.

$$OCV_d(SoC) = a_1 + a_2 \cdot \frac{1}{1+e^{a_3\cdot(SoC-a_4)}} + \\ + a_5 \cdot \frac{1}{1+e^{a_6\cdot(SoC-a_7)}} + a_8 \cdot \frac{1}{1+e^{a_9\cdot(SoC-1)}} + \\ + a_{10} \cdot \frac{1}{1+e^{a_{11}\cdot SoC}} + a_{12} \cdot SoC \quad (19)$$

where the subscript *d* stands for discharge and the indexed coefficients values are given in Table I:

TABLE I. THE VALUES OF OCV(SOC) COEFFICIENTS FOR DISCHARGE

a_1	3.42	a_4	1.051	a_7	0.22	a_{10}	-0.8151
a_2	154.5	a_5	0.05668	a_8	-0.229	a_{11}	46.48
a_3	-140.8	a_6	-21.15	a_9	167.8	a_{12}	0.0891

V. EKF INTRINSIC BEHAVIOR DURING OPERATION

The operation of the Kalman filter resembles in some way that of a negative feedback operational amplifier: it keeps adjusting its internal parameters such that the estimated response of the system/battery fits the measured one. This mechanism depicts the negative feedback of the filter: when the estimated and measured battery terminal voltages fit together, the correction step impact on the state vector will be insignificant due to the contracting innovation term in (13), analogue to the differential voltage at the inputs of the op-amp. As shown in Fig. 13, except for the inceptive fragment and the load transients, the innovation term is approaching zero. As part of the state vector, the estimated state-of-charge is directly affected by the reduction of the innovation term.

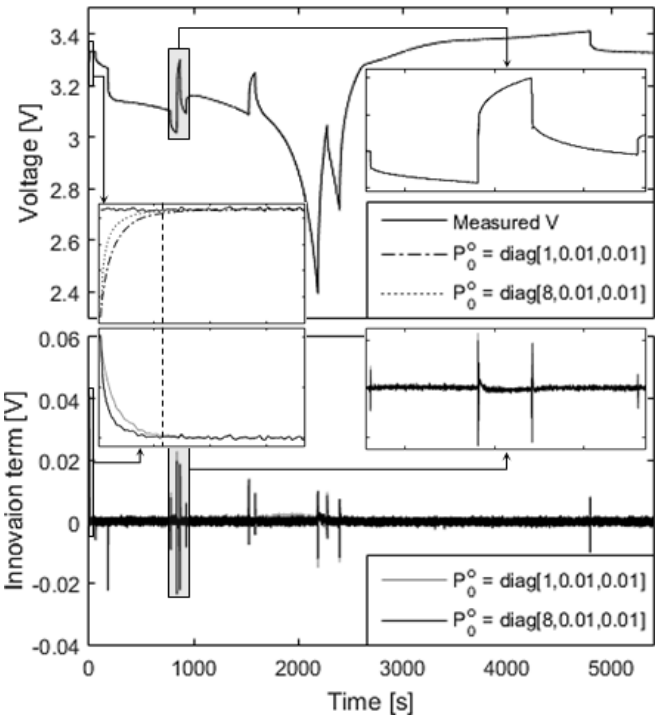

Figure 13. Dynamics of the innovation term during a random load profile (left zoom – initial convergence, right zoom – behavior during load transients)

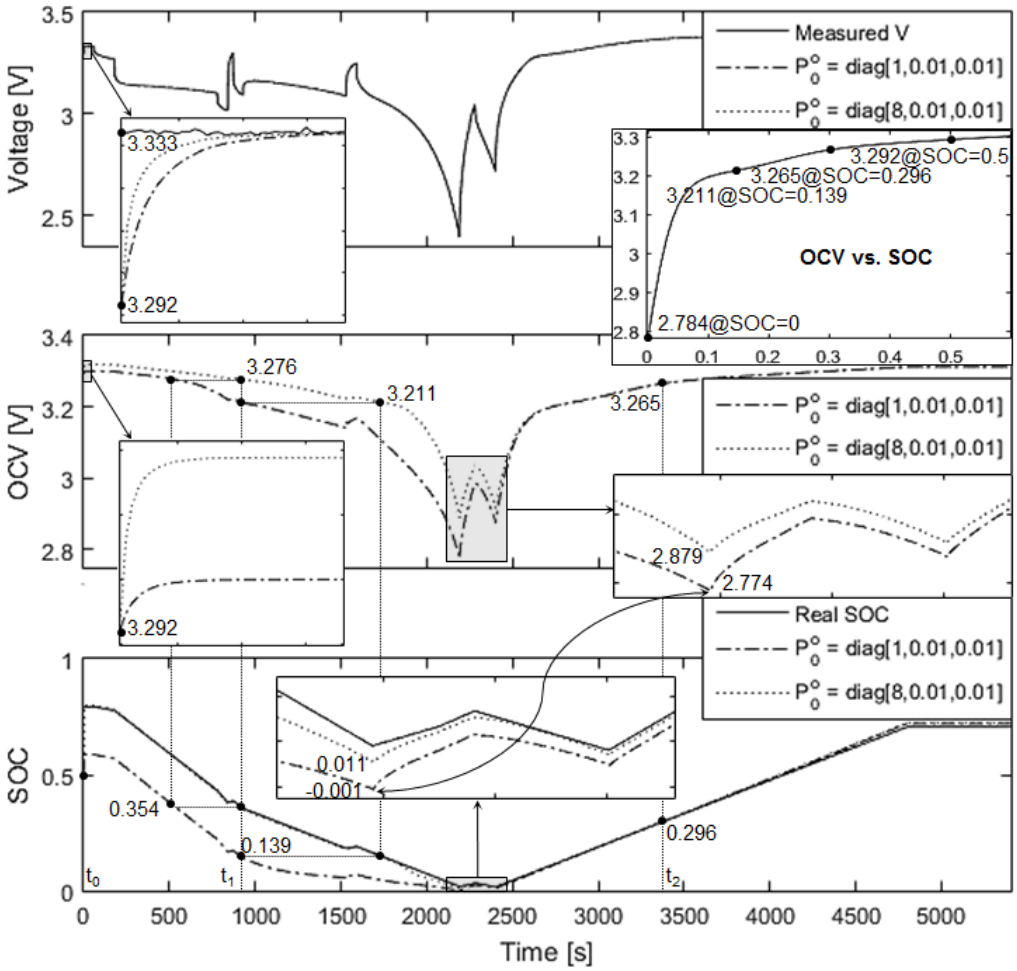

Figure 14. Evolution of the implemented EKF for two different P^o_0 (random profile applied to a pre-discharged cell)

Fig. 14 reveals in a graphical manner the evolution of the filter when initialized with two distinct error covariance matrices: as one can notice, the incipient OCV and terminal voltage estimations are similar in both cases (i.e. 3.292 V) and correspond to a loading state of 0.5 – the two values are given by the employed OCV vs. SoC relationship in (19) which is illustratively represented by the OCV vs. SoC inset.

Once the calculated terminal voltage approaches the measured one, the theoretical SoC will no longer converge towards the real value and the estimation algorithm will closely track the OCV vs. SoC function – the 0.139 of SoC corresponds to an OCV value of 3.211 V according to (19), which is also reflected in the resulted OCV waveforms. The SoC traces meet near the depletion point. Unlike the voltage gap between the OCV signals, which is still significant, its SoC correspondent is much narrower, since the OCV curve is changing dramatically in the extreme SoC regions. After merging, the two estimates will track firmly the real SoC for a while, but will softly start to drift away during the last charge event (the kickoff point of the scattering is around 0.3 of SoC).

Table II provides further explanations on Fig. 14: the first row emphasizes the close connection between the initial values of the estimated battery terminal voltage, V_{t_est}, and OCV, due to requisite filter initialization at t_0. The first value of the two calculated voltages is similar, being given solely by the initial value of the SoC as the voltage drop across the RC branches is considered zero (15). On the other hand these values differ from the real signal, V_{t_meas}, as the filter did not have the time to converge towards the real signal (the negative feedback did not come into play yet).

TABLE II. DYNAMICS OF IMPLEMENTED EKF (RELATIVE TO FIG. 14)

OCV vs. SoC (19)			**P^o_0=diag[1,0.01,0.01]**			**P^o_0=diag[8,0.01,0.01]**	
SoC	**OCV**	**V_{t_meas}**	**SoC**	**OCV**	**V_{t_est}**	**OCV**	**SoC**
0.5	3.292	3.333	0.5	3.292	3.292	3.292	0.5
0.354	3.276	-	-	-	-	3.276	0.354
0.139	3.211	-	0.139	3.211	-	-	-
0	2.784	-	-0.001	2.774	-	2.879	0.011
0.296	3.265	-	0.296	3.265	-	3.265	0.296

The next two rows in the table approach the t_1 moment, separately for each variant of P^o_0, as the two SoC traces differ significantly from each other at that time instant. Taking a closer look on the cell values reveals one fundamental aspect of the EKF operation: the estimated SoC value is a strong function of calculated OCV. Although different, the two estimates returned approximately similar SoC values corresponding to identical OCV magnitudes (see dashed connection lines inside Fig. 14). The value of the battery terminal voltage was registered only for the first step, as the three waveforms plotted in the upper window (i.e. the measured one and the two computed by the filter) overlay for the rest of the simulation profile. Finally, the last two rows are more or less similar, as the real and the estimated signals match closely. The dashed cells were considered not relevant for this explanation.

Fig. 15 depicts the individual voltage contribution of the ECM branches to the calculated OCV value. The voltage drop across each branch is strongly influenced by the value of the associated circuit elements as a function of SoC. This

can be easily noticed in the upper section of the figure: the two voltage waveforms are dissimilar for a good part of the load profile, although the same current pattern is applied. This is because of different values of internal resistance, R_0, corresponding to distinct loading states of the battery. Though not as intuitive as in the case of the purely resistive component, the same is valid for the other two RC branches. Once the two SoC estimations fit to each other, the computed voltage traces are matching closely.

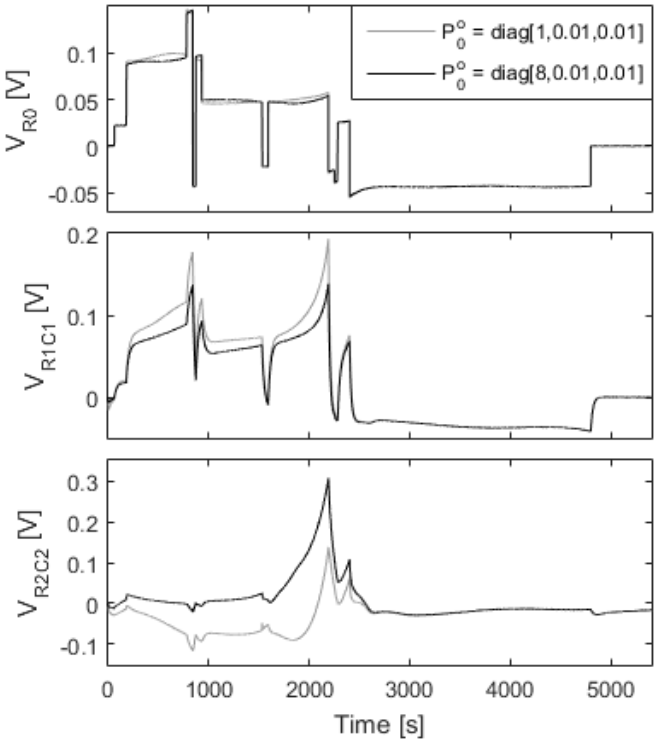

Figure 15. The estimated voltage drops across the ECM branches

Further on, a graphical representation of (2) is given in Fig. 16, considering a discharge current pulse applied to a fully rested cell (i.e. the OCV and terminal voltage, V_t, overlap just before the load pulse is applied).

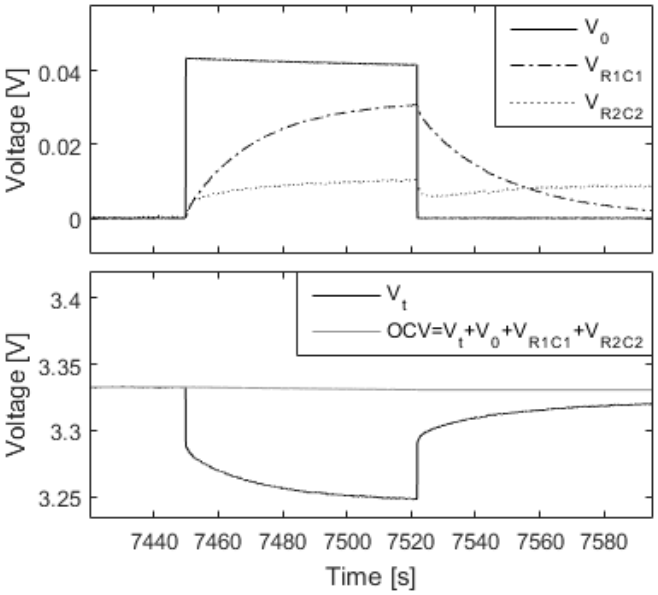

Figure 16. Graphical representation of (2) for a discharge current pulse

The top window in Figure 16 depicts the arrangement of the three voltage signals calculated for each passive branch of the circuit model: R_0, R_1C_1 and R_2C_2. The computation of the three waveforms is done in such a way that the resulted terminal voltage fits the measured one. The bottom section of the figure displays the calculated terminal voltage, V_t, and the resulted OCV after (2) is applied.

VI. EKF VS. NONLINEARITY

A closer look on the evolution of the Kalman gain unveils a rather unexpected behavior: unlike the innovation term, which displays no sharp transitions during stationary load regimes, the elements of the Kalman gain matrix exhibit a peculiar oscillation, with no apparent link to the load transients:

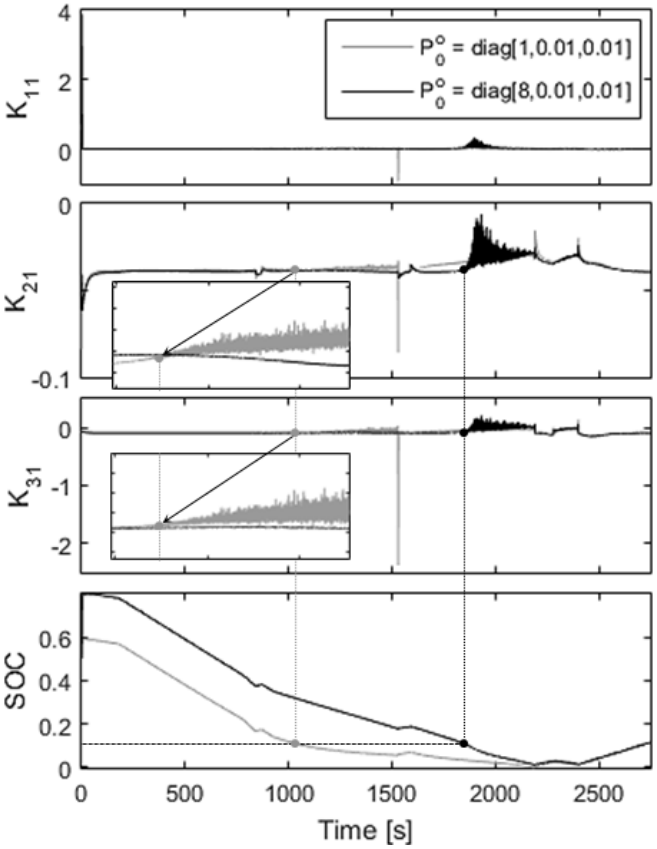

Figure 17. Numerical oscillation within the elements of the Kalman gain matrix

According to Fig. 17, the 'noisy' behavior of the Kalman gain matrix, is deterministic and starts when entering the 0.1 – 0 SoC region. The same behavior is valid within the 1 – 0.95 SoC range. Both intervals correspond to the highly nonlinear sections of the OCV vs. SoC characteristic of the lithium cell.

Fig. 18 provides an additional explanation of the phenomenon discussed above. As already pointed out, the Kalman gain oscillations occur over the highly nonlinear regions of the OCV vs. SoC curve. This fact is highlighted by the plot of the first derivative of the OCV as a function of SoC, which poses an abruptly increasing trait reflecting the strong nonlinear dynamics of the OCV. The root cause of this phenomenon lies within the elements of the error covariance matrix. Over these regions the first order Taylor approximation performs poorly and hence the estimation precision is altered (viewed solely from the nonlinearity standpoint) increasing the value of these elements. The noise effect is amplified by the multiplication of the matrix by the transpose of C_k (C_k is the Jacobian matrix containing the

derivative of OCV as a function of SoC element), when computing the Kalman gain matrix in (12). Further on, the hum will propagate cyclically through the filter.

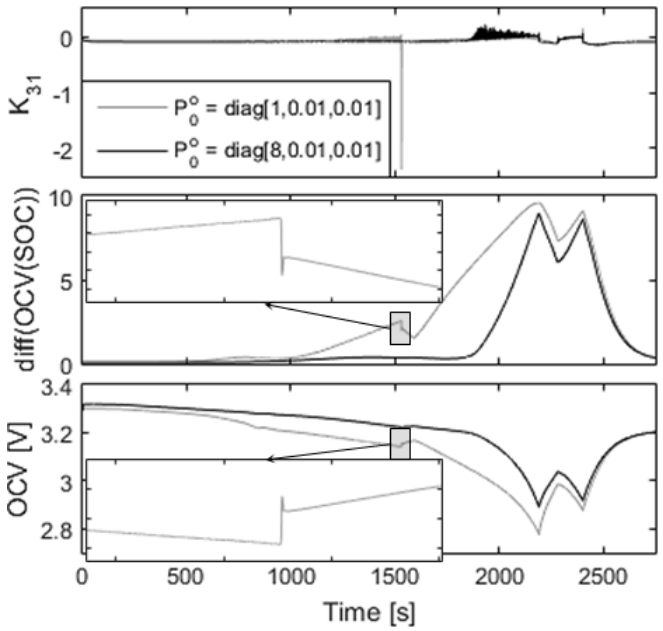

Figure 18. Illustration of the linkage between OCV nonlinearity and the numerical oscillations of the Kalman gain

Another uncommon appearance within the elements of the Kalman gain matrix is represented by the short dip for $P^{o}_{0}=diag[1,0.01,0.01]$. This is correlated with an abrupt change of the computed OCV signal, also reflected by the steep front, approaching infinity, of its derivative with respect to SoC, as shown by the stretched insets of Fig. 18. The overturn of the OCV signal was triggered by a sudden polarity change into the load current profile inside the nonlinear OCV region.

VII. CONCLUSION

Whereas an EKF represents a common approach for handling nonlinearities, its intrinsic behavior is rather intricate and hard to analyze. This paper depicts the operation of the EKF from a different point of view, offering an intuitive way to comprehend the elaborate mechanism behind the filtering process by visualizing the evolution of its internal parameters on a practical application. The physical model of the system (i.e. the ECM) is regarded as the backbone of the estimator, impacting the capability of the algorithm to accurately track the real data. As the complexity of the model and the filter performance are positive covariant features, an adaptive model was chosen for this application to keep track of the model parameters over the entire SoC range. Fine-tuning challenges were treated separately, as method and application specific. An analogy between the negative feedback in the popular operational amplifier and the similar behavior of the Kalman filter was made to allow better understanding of the internal gain evolution. The output function of the filter was graphically represented, taking into account the dependence between the components of the model and estimated SoC. Finally, the paper pointed out some peculiarities of the EKF parameters caused solely by the nonlinear behavior of the managed systems.

REFERENCES

[1] M. van der Steen, R. M. van Schelven, R. Kotter, M. J. W. van Twist and P. van Deventer, "EV policy compared: An international comparison of governments' policy strategy towards e-mobility," in E-Mobility in Europe, Springer International Publishing, Switzerland, 2015, pp. 27-53, doi: 10.1007/978-3-319-13194-8_2

[2] D. Doughty and E. P. Roth, "A general discussion of Li ion battery safety," The Electrochemical Society Interface, vol. 21, no. 2, pp. 37-44, Summer 2012, doi: 10.1149/2.F03122if

[3] D. A. Corrigan and A. Masias, "Batteries for electric and hybrid vehicles," in Linden's Handbook of Batteries, T. B. Reddy, 4th ed., New York: McGraw-Hill, 29.2 EV Battery Performance Targets, 2011.

[4] D. Belov and M. H. Yang, "Investigation of the kinetic mechanism in overcharge process for Li-ion battery," Solid State Ionics, vol. 179, no. 27-32, pp. 1816-1821, Sept. 2008, doi: 10.1016/j.ssi.2008.04.031

[5] H. Maleki and J. N. Howard, "Effects of overdischarge on performance and thermal stability of Li-ion cell," Journal Power Sources, vol. 160, no. 2, pp. 1395-1402, Oct. 2006, doi: 10.1016/j.jpowsour.2006.03.043

[6] H. Rahimi-Eichi, U. Ojha, F. Baronti and M.-Y. Chow, "Battery management system: an overview of its application in the smart grid and electric vehicles," IEEE Industrial Electronics Magazine, vol. 7, no. 2, pp. 4-16, June 2013, doi: 10.1109/MIE.2013.2250351

[7] K.-S. Ng, Y.-F. Huang, C.-S. Moo and Y.-C. Hsieh, "An enhanced coulomb counting method for estimating state-of-charge and state-of-health of lead-acid batteries," Intl. Telecommunications Energy Conf., Dec. 2009, doi: 10.1109/INTLEC.2009.5351796

[8] H. Dai, Z. Sun and X. Wei, "Online SOC estimation of high-power lithium-ion batteries used on HEVs," in ICVES, June 2007, pp. 342-347, doi: 10.1109/ICVES.2006.371612

[9] H. He, R. Xiong, X. Zhang, F. Sun and J. Fan, "State-of-charge estimation of the lithium-ion battery using an adaptive extended Kalman filter based on an improved Thévenin model," IEEE Trans. Vehicular Technology, vol. 60, no. 4, pp. 1461-1469, May 2011, doi: 10.1109/TVT.2011.2132812

[10] Q. Yu, R. Xiong, C. Lin, W. Shen and J. Deng, "Lithium-ion battery parameters and state-of-charge joint estimation based on H infinity and unscented Kalman filters," IEEE Trans. Vehicular Technology, doi: 10.1109/TVT.2017.2709326, to be published.

[11] Y. Wang, H. Fang, L. Zhou and T. Wada, "A methodical investigation of the extended Kalman filter approach," IEEE Control Systems Magazine, vol. 37, no. 4, pp. 73-96, July 2017, doi: 10.1109/MCS.2017.2696761

[12] Y. Niu and L. Hu, "An extended Kalman filter application on moving object tracking," in Proc. 5th Intl Conf. Electrical Engineering and Automatic Control, Springer, Berlin, Heidelberg, 2016, pp. 1261-1268, doi: 10.1007/978-3-662-48768-6_141

[13] R. Faragher, "Understanding the basis of the Kalman filter via a simple and intuitive derivation," Signal Processing Magazine, vol. 29, no. 5, pp. 128-132, Sept. 2012, doi: 10.1109/MSP.2012.2203621

[14] T. Michalski, C. Lopez, A. Garcia and L. Romeral, "Sensorless control of five phase PMSM based on extended Kalman filter" Annual Conf. IEEE Industrial Electronics Society, Oct. 2016, pp. 2904-2909, doi: 10.1109/IECON.2016.7793740

[15] G. L. Plett, "Extended Kalman filter for battery management systems of LiPB-based HEV battery packs, Part1. Background," Journal Power Sources, vol. 134, no. 2, pp. 252-261, June 2004, doi: 10.1016/j.jpowsour.2004.02.031

[16] O. B. Belghith, L. Sbita and F. Bettaher, "Maximum power point tracking by the technique of the extended Kalman filter" in GECS, Oct. 2017, doi: 10.1109/GECS.2017.8066198

[17] A. A.-H. Hussein and I. Batarseh, "An overview of generic battery models," IEEE Power and Energy Society General Meeting, July 2011, doi: 10.1109/PES.2011.6039674

[18] F. Ciortea, C. Rusu, M. Nemes and C. Gatea, "Extended Kalman filter for state-of-charge estimation in electric vehicle battery packs," in OPTIM, May 2017, pp. 611-616, doi: 10.1109/OPTIM.2017.7975036

[19] F. Ciortea, S. Hintea, C. Gatea and M. Nemes, "Measurement method and parametric modelling of $LiFePO_4$ cell for SOC estimation in EVs," in OPTIM, May 2017, pp. 675-680, doi: 10.1109/OPTIM.2017.7975046

[20] R. M. Mehra, "On the identification of variances and adaptive Kalman filtering," IEEE Trans. Automatic Control, vol. AC-15, no. 2, pp. 175-184, Apr. 1970, doi: 10.1109/TAC.1970.1099422

[21] W. Ding, J. Wang and C. Rizos, "Improving adaptive Kalman estimation in GPS/INS integration," The Journal of Navigation, vol. 6, no. 3, pp. 517-529, Aug. 2017, doi: 10.1017/S0373463307004316